Composite Structures 234 (2020) 111698

Contents lists available at ScienceDirect

Composite Structures

journal homepage: www.elsevier.com/locate/compstruct

Prediction of shear strength and behavior of RC beams strengthened with externally bonded FRP sheets using machine learning techniques

Omar R. Abuodeh, Jamal A. Abdalla*, Rami A. Hawileh

Department of Civil Engineering, American University of Sharjah, United Arab Emirates

ARTICLE INFO

Keywords:
Neural network
Machine learning
Recursive feature elimination
FRP shear strength
Side-bonded
U-wrapped

ABSTRACT

This paper presents the use Machine Learning (ML) techniques to study the behavior of shear-deficient reinforced concrete (RC) beams strengthened in shear with side-bonded and U-wrapped fiber-reinforced polymers (FRP) laminates. An extensive database consisting of 120 tested specimen and 15 parameters was collected. The resilient back-propagating neural network (RBPNN) was used as a regression tool and the recursive feature elimination (RFE) algorithm and neural interpretation diagram (NID) were employed within the validated RBPNN to identify the parameters that greatly influence the prediction of FRP shear capacity. The results indicated that the RBPNN with the selected parameters was capable of predicting the FRP shear capacity more accurately (r^2 = 0.885; RMSE = 8.1 kN) than that of the RBPNN with the original 15 parameters (r^2 = 0.668; RMSE = 16.6 kN). The model also outperformed previously established standard predictions of ACI 440.R-17, *fib*14 and CNRDT200. A comprehensive parametric study was conducted and it concluded that the implementation of RBPNN with RFE and NID, separately, is a viable tool for assessing the strength and behavior of FRP in shear strengthened beams.

1. Introduction and background

Externally strengthening reinforced concrete (RC) structures has been a popular practice in both the industry and research community over the last few decades [1–5]. This application involves bonding composites to the surfaces of RC members to upgrade their strength, stiffness, and ductility [6–8]. In particular, experimental investigations have been conducted to study the shear behavior of RC beams externally strengthened using composites like carbon-fiber reinforced polymers (CFRP), glass fiber-reinforced polymers (GFRP), aluminum alloy (AA) plates, and high strength steel wires [1,9–14]. Other studies involved different shear strengthening schemes, where the major schemes that have been implemented in the literature were FRP U-wrapped and side-bonded sheets/strips [1,4,7,15]. This encouraged the development of empirical models for predicting the design shear strength of RC beams externally strengthened using bonded FRP sheets/strips [16,17]. All developed models, very much, follow the same concept where the ultimate shear capacity of an externally strengthened RC beam is the summation of the shear contribution from concrete (V_c), steel (V_s), and FRP (V_f).

Furthermore, this concept assumes that the beam's shear force components reach their peak values without one component failing prior to the other. It overestimates the shear strength and does not account for any shear interaction between the different shear force components explained earlier [17]. Chen et al. [17] published an article about the shear interaction-effect between FRP strips (U-wrapped and side bonded) and internal steel stirrups. A design shear capacity model for FRP shear-strengthened RC beams was developed in which the effects of the size, spacing, and yield strength of the steel stirrups on the FRP contribution in shear were considered. Their findings represented a valuable step forward in the literature; however, the model development does not account for crack-width variations that are dependent on: (a) the amounts of steel and FRP shear reinforcement; (b) tensile reinforcement. Another study was conducted by Colotti and Swamy [18], where an analytical model was developed to estimate the shear contribution of FRP reinforcement, by assessing the flexural-shear interaction between the internal steel reinforcement and external FRP reinforcement. As a result, the model is capable of evaluating the shear capacity of FRP-strengthened RC beam with sufficient accuracy and reliability. However, its mathematical structure is lengthy and somehow complicated since it analytically accounts for various cases such as: (a) flexural-shear interaction failure modes including the contribution of external shear reinforcement, FRP debonding, and FRP rupture; (b) shear web-crushing; (c) pure flexural failure modes.

With the advancement in soft computing, machine learning (ML) methods have been utilized to identify and address civil engineering

* Corresponding author.
E-mail addresses: oabuode@g.clemson.edu (O.R. Abuodeh), jabdalla@aus.edu (J.A. Abdalla), rhaweeleh@aus.edu (R.A. Hawileh).

https://doi.org/10.1016/j.compstruct.2019.111698
Received 20 August 2019; Received in revised form 8 November 2019; Accepted 12 November 2019
Available online 16 November 2019
0263-8223/

problems [18–21]. Artificial Neural Network (ANN), is a computational paradigm that mimics the human brain by receiving *inputs* and iteratively maps them into an arbitrary number of matrices. This process is repeated until the model minimizes the error and accurately approximates a solution. By utilizing the regression nature of this tool, civil engineers have executed it to produce dynamic models that evaluate the response variables [22]. ANN was also used in a variety of studies which involved investigating the nonlinear behavior of concrete structures [18,22,23]. Recently, researchers have implemented ANN to accurately predict the shear capacity of RC beams that are strengthened using composite materials [24]. Other retrofitting applications involving the confinement effect of composite materials on the axial-load capacity of RC columns were also investigated using ANN [25–27]. ANN has also been successful in modeling FRP debonding by identifying the parameters that directly influence this failure mode [28].

However, a drawback of implementing ANN is its black-box nature that offers little tangible insight of how the model analyzes the independent parameters. This drawback can be partially eliminated by using variable importance methods which incorporate ML models. Common ML tools used extensively in the published literature are Sequential Feature Selection (SFS) [36] and Neural Interpretation Diagram (NID). These algorithms assist the user in identifying the parameters that significantly influence the model and thus understand the behavior of the model. For instance, Rodriguez Galiano et al. [29] used SFS methods to select the most important features within subset of 20 parameters in predicting groundwater pollution. As a result, the final model with the selected features yielded the most accurate results. Mozumder, and Laskar [30] employed the NID to study the viability of ANN in predicting unconfined compressive strength of geo-polymer stabilized clayey soil. The study focused on studying 283 soil samples by feeding them as inputs into an ANN, and predicting the strength of soil. The trained ANN incorporated a NID to perform a sensitivity analysis and identify the most influential features that affect the model. As a result, the liquid limit and the plastic limit resulted in negative effects on the ANN model while the other parameters showed positive association with the ANN model.

Recently, two studies were conducted by the authors of this paper to investigate the viability of implementing ANN with NID to accurately predict the FRP shear resistance in externally strengthened RC beams, and ANN with SFS to accurately predict the compressive strength of ultra-high performance concrete [31,32]. This encouraged the implementation of a more confident framework such that recursive feature elimination (RFE), a sister tool of SFS, with NID can be utilized to identify and select the critical parameters in a model. The aim of this study is to implement ML algorithms with a validated ANN to identify the critical parameters which affect the accuracy of predicting the FRP shear capacity of strengthened RC beams with FRP laminates and obtain a rational model. An extensive database of 120 points with 15 variables was compiled from the published literature, where the geometric and mechanical properties of concrete, internal steel reinforcement, and FRP strips/sheets were accounted for. The selected parameters were carefully studied and compared to published experimental works to validate the model's consistency. Predictions were made using the model with the selected features and compared to the predictions calculated using previously established models found in international design codes and standards (ACI 440.R-17; fib14; CNRDT200). Finally, a comprehensive parametric study was conducted to investigate the effect of FRP and internal transverse steel reinforcement on the FRP shear capacity of shear-strengthened RC beams. The findings of this study could assist structural engineers and researchers in implementing emerging ML tools in simulating the shear behavior of externally strengthened RC beams.

2. Research significance

The previously mentioned models [17,18] follow the truss analogy in which a list of failure modes is assumed to derive different expressions. This produces a network of discrete models whose complexity increases as the number of assumptions increases; hence, arriving at an impractical model that is difficult to use in design. Therefore, developing analytical models using the truss analogy, alone, imposes certain restrictions and is somehow lengthy and complicated. In addition, several experimental investigations involving an extensive variation in parameters were conducted in the literature. These extensive databases should be utilized in emerging computational toolboxes (i.e., ANN, RFE, and NID) to accommodate the dynamic nature of the system, while maintaining a simple model.

3. Methodology

3.1. Resilient back propagation neural network

Another AI tool that is a modified version of ANN is the resilient back-propagation neutral network (RBPNN), where both algorithms tweak the biases and weights such that the model locates a local minimum in the error or *loss* function [33]. By taking the partial derivative of the loss function in terms of the weights (dE/dω), it is possible to know the direction of the local minimum in a function and manipulate the initial weights. The underlying differences between the BPNN and RBPNN algorithms are: (a) the RBPNN imposes a unique learning rate, η_k, for every weight in the ANN model as opposed to the BPNN algorithm, which uses a learning rate to the overall model; (b) when calculating the next weights of the model, the BPNN algorithm accounts for both the sign and magnitude of the partial derivative, whereas the RBPNN uses only the sign such that the learning rate mainly influences the convergence of the model. Equation (1) summarizes the RBPNN algorithm in the ANN, where t is the iteration step and k represents the weight between the connected neurons. In this study, the Resilient Back Propagation Neural Network (RBPNN) was employed as a wrapper for another machine learning tool called neural interpretation diagram (NID), which will be discussed in the following sections.

$$\omega_k^{t+1} = \omega_k^t - \eta_k \cdot sign \cdot \left(\frac{\partial E^{(t)}}{\partial \omega_k^{(t)}} \right) \tag{1}$$

The accuracy of an ANN model is highly dependent on the nature of the data it analyzes. To avoid overfitting and obtaining inaccurate predictions, the input data points need to be *scaled* between a comparable range of numbers and aim for a smoother relationship, noise reduction, and feature extraction. There are several scaling techniques in the literature that map the data points to a certain domain of numbers, which include: the min-max normalization, the Z-score normalization, and the sigmoidal normalization. In this study, the min-max normalization was used to map the parameters between a domain, [0,1], as presented in Equation (2). The min-max normalization scaling technique simplifies the ML tools since all of the parameters are within the same scale; making it easier to compare and become more robust.

$$z_i = \frac{x_i - \min(x_i)}{\max(x_i) - \min(x_i)} \tag{2}$$

The matrix multiplication that occurs within the hidden layers is accompanied with an *activation* function that transforms the calculated set of results into a particular domain of numbers. The most popular activation functions used in regression and classification analyses are: (a) sigmoid function; (b) hyperbolic tangent function; (c) linear activation functions. In this study, the sigmoid function was used repeatedly between the hidden and outputs layers, and the linear activation function was used to transform the final predictors to the linearized form. Equation (3) and Equation (4) presents these activation functions, where F is the function containing variable X. The sigmoid activation function maps the products of the hidden layers between 0 and 1 while maintaining its nonlinear form, which simplifies the ANN

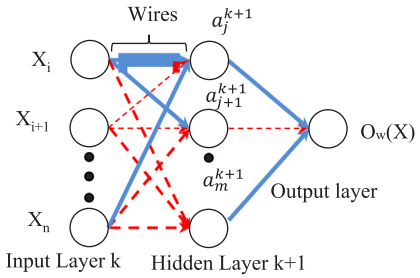

Fig. 1. NID Architecture.

and makes it more versatile.

$$f = \frac{1}{1 + e^{-F(X)}} \tag{3}$$

$$f = F(X) \tag{4}$$

3.2. Neural interpretation diagram

Researchers have advocated the usage of ML tools to visually inspect the magnitude of the ANN's weights and interpret the input variables' contributions in the ANN model [34,35]. Neural interpretation diagrams (NID) provide a visual representation of the positive (high influence) and negative (low influence) weights using different highlighted colors on the ANN model's wires. Fig. 1 shows a single hidden layered NID with blue and red colored wires, where both the blue (solid) and red (dashed) colors represent a positive (high influence) and negative (low influence) association between the input and output variables, respectively. Interpreting connection weights of NIDs, alone, is difficult due to the complexity of connections among the neurons. Therefore, Olden and Jackson [35] proposed a Randomization test that quantifies the input variable's contributions and constructs multiple ANN models, with different initial random weights. Afterwards, the most accurate ANN model is selected and the initial weights are used to estimate the relative importance, using the Garson's algorithm. As a result, a histogram is generated to illustrate the frequency of positive associations (high influence) corresponding to each input parameter. This method empirically constructs the relationships between the input and output parameters, which precludes the physical soundness of the ANN model and forced it to over fit. To alleviate this, another variable importance ML algorithm should be used to validate the results produced by the NID.

3.3. Recursive feature elimination

Another ML tool that identifies the most influential parameters within a model is the *Recursive Feature Elimination* (RFE) function. RFE is an optimization technique that aims to find the most contributing independent parameters within a dataset of distinct parameters during regression. It is employed with a wrapper, the RBPNN, to repeatedly create models by recursively appending input parameters to the model during each run until the error drastically increases. In this study, the Root Mean Square Error (RMSE) was used to evaluate the error between the model and the measured values. The RFE works by systematically removing input parameters until the error is minimized and a dataset filled with the independent parameters is obtained. Afterwards, it ranks the selected features based on the order of their elimination. A summary of the RFE algorithm is shown in Fig. 2.

4. Experimental data: collection, classification and validation

Extensive research has been conducted in studying the nonlinear behavior of externally strengthened RC beams, in shear, using ANN models [15–17]. Geometric properties, reinforcing steel, and externally bonded reinforcement (EBR) details were used as input parameters for predicting the shear contribution of the EBR. Table 1 presents a brief summary of studies that have used ANN for selected shear strengthening techniques along with the corresponding parameters employed in those studies.

Perera et al. [40] and Narderpour et al. [38] used ANN to predict the shear strength of RC beams and compared their predications with analytical/empirical prediction models from different design codes and standards. They also carried out sensitivity analyses using the Garson Index to determine the relative importance of each input parameter with respect to the shear contribution of FRP. The results showed that the developed ANN models were capable of accurately predicting the FRP shear contribution by a larger margin than the analytical/empirical models obtained from different international codes and standards. Similarly, Perera et al. [40] incorporated AI models like genetic algorithm and ANN to investigate the shear mechanism of strengthened RC beams. As a result, the work presented two AI models, GA and ANN, which outperformed the analytical/empirical models obtained from international design codes and standards in predicting the shear strength of externally strengthened beams.

In this study, a database of 120 points and 15 variables consisting of the geometric and mechanical properties of shear-strengthened RC beams was collected from the published literature. These data points varied based on their individual mechanical and geometric properties, in which the authors followed a predefined criteria such that over-fitting and inaccurate predictions could be avoided. This predefined data search criteria is described below:

- Normal-sized rectangular and T-shaped RC beam sections were collected, where the span exceeds four times the depth of the section or the shear span-to-depth ratio is greater than two (a/d > 2) in accordance with the ACI 318-14 code [44].
- Both four-point and three-point loading schemes were accounted for.
- The collected specimens were made up of both normal strength and high strength concrete.
- The presence and absence of transverse steel reinforcement, with its corresponding spacing, was accounted for.
- The materials used, in shear strengthening, were fiber-reinforced polymers (FRP); mainly carbon FRP (CFRP) and glass FRP (GFRP).
- The strengthening techniques of the collected specimens were focused on U-wrapped and side-bonded (SB) RC beams.
- The specimens consisted of spaced and continuous strips.
- The shear capacity of the FRP retrofit was assumed to be the difference between the ultimate shear force resisted by the strengthened sample and the shear force resisted by the control sample.

The parameters included in this study were similar to the parameters studied by previous authors, as shown in Table 1. However, some parameters, like ratio of both steel and fiber, are functions of other independent parameters. Therefore, each parameter used in this study was completely independent to investigate the behavior of each parameter individually. Table 2 outlines the statistical measurements of these collected specimens. It is worth mentioning that a value of 0 in the yield strength of the steel stirrups ($f_{y,s}$) and area of stirrup-to-spacing ratio (A_v/S) indicates no internal shear reinforcement in the tested beams. Also, a value of 0 in the area of longitudinal reinforcement (A_{st}) and width of FRP U-wrap (B_f) indicates that there was no longitudinal reinforcement and U-wrap strength, respectively, in the tested beams.

Prior to the ANN analysis, the statistical measurements of the data were evaluated to understand the spread of the points and remove any outliers that would hinder the analysis. This can be achieved by visually inspecting these statistical measurements in Table 2, where most of the parameters have similar medians and means. Fig. 3 presents a graphical representation of this particular distribution, where the authors

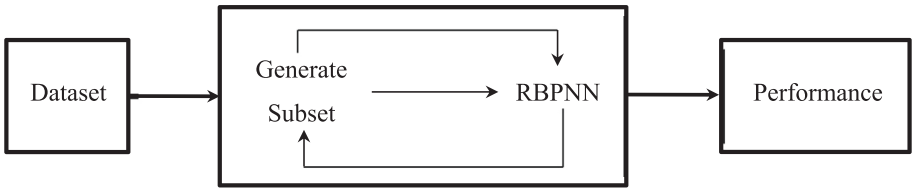

Fig. 2. RFE Flowchart.

Table 1
Studied input parameters for selected strengthened RC beams in shear by different authors.

Author		Tanarslan et al. (2012) [37]	Li et al. (2017) [42]	Perera et al. (2016) [40]	Perera et al. (2016) [41]	Naderpour et al. (2017) [38]	Adhikary et al. (2004) [39]	Yousif et al. (2010) [24]
Concrete Details	b_w (mm)	√	√	√	√		√	√
	d_{eff} (mm)	√	√			√	√	√
	h (mm)			√	√			√
	L (m)							√
	a/d	√	√			√	√	√
	f_c (MPa)	√	√	√	√	√		√
Reinforcement Details	ρ_L				√		√	
	$\rho_{T,90}$						√	
	$A_{T,90}$ (mm^2/mm)			√	√			√
	$A_{L,B}$ (mm^2)							√
	$A_{L,T}$ (mm^2)		√					√
	f_{yT} (MPa)			√	√		√	√
Externally Bonded Reinforcement Details	w_f/s_f	√	√			√		√
	β (^{0})	√		√	√	√		
	t_f (mm)	√	√			√	√	√
	ρ_f			√	√			
	d_f (mm)					√		√
	h_f/h_B						√	
	E_f (MPa)	√	√	√	√	√		√
	ε_{fu}	√	√			√		
	f_{fu} (MPa)						√	√

attempted to obtain a normal or ideal distribution for all parameters. However, due to the broad spectrum of variables that were studied, a perfectly bell-shaped distribution was not obtained. These drawbacks could hinder the model's accuracy of predicting the shear strength, and forced the authors to cut down on any outliers without benefitting the model. Therefore, ML methods should be used to efficiently remove the independent parameters that negatively influence the model's performance.

5. Artificial selection process

5.1. Validating RBPNN architecture

In this study, the RBPNN was constructed as a wrapper for both the NID and RFE algorithm; however, its structure is created by defining the number of hidden layers and neurons in the network. This was accomplished by implementing a trial-and-error approach and automatically adding one neuron per analysis for a total of 15 neurons. During each analysis, the data points are divided into the following: (a) 70% for training; (b) 15% for validation; (c) 15% for testing. This separation of data prevents the model from memorizing the solution and makes it more reliable. Fig. 4 shows the neuron-validation process for selecting the optimum number of neurons required for the model to predict the most accurate outputs. It is worth mentioning that for each neuron inserted ten analyses were executed and the average RMSE was assigned to the selected neuron. As a result, 8 neurons were sufficient enough to yield an average RMSE value of about 90 kN.

A double hidden layered RBPNN was also tested in which the

Table 2
Statistical Measurements of the Experimental data.

Parameters	Symbols	Minimum	1st Quartile	Median	Mean	3rd Quartile	Maximum	Standard Deviation
Beam width (mm)	b_w	75	75	150	144.6	150	250	40.7
Depth (mm)	d_{eff}	118	118	270	263.5	343	425	84.3
Length (m)	L	0.5	0.5	2	2.3	3	4.52	1.0
Span-to-depth ratio (mm/mm)	a/d	2.5	2.52	2.78	2.7	3	6	0.8
Compressive strength of concrete (MPa)	f_c	13.3	13.3	34.7	35.7	41.8	61	10.0
Yield strength of stirrups (MPa)	$f_{y,s}$	0	0	252	235.3	441	645	222.5
Area of stirrups-to-spacing ratio (mm^2/mm)	A_v/S	0	0	0.1885	0.3	0.503	1.57	0.4
Yield strength of longitudinal reinforcement (MPa)	$f_{y,L}$	391	391	464	473.1	500	759	65.5
Area of longitudinal reinforcement (mm^2)	A_{st}	0	0	11,093	45,958	73,095	375,406	66,469
Thickness of FRP sheet (mm)	t_f	0.1	0	0.167	0.3	0.33	2.1	0.4
Width of FRP U-Wrap (mm)	B_f	0	0	120	103.5	150	250	67.3
Height of FRP strip (mm)	H_f	25	25	300	261.7	305	450	88.4
Width of FRP-to-FRP strip spacing (mm/mm)	W_f/S_f	0.05	0.05	1	0.8	1	1	0.3
Ultimate strength of FRP (MPa)	f_f	160	160	3450	2937	3650	4361	1222
Modulus of elasticity of FRP (GPa)	E_f	5.79	5.79	230	197.8	231	390	92.7
FRP shear capacity (kN)	V_f	10	10	30.5	33.4	42.5	91	17.8

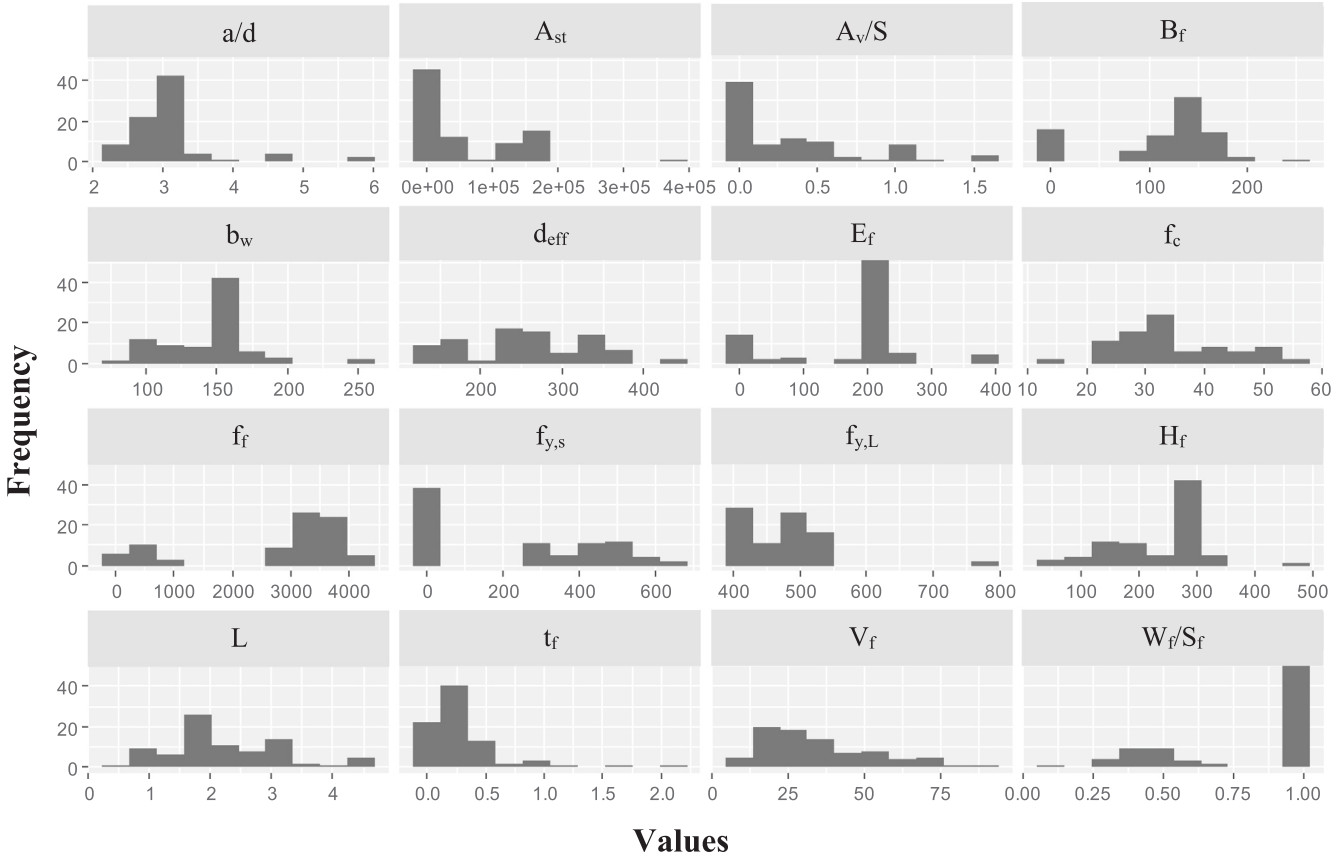

Fig. 3. Histogram Plots of Collected Parameters.

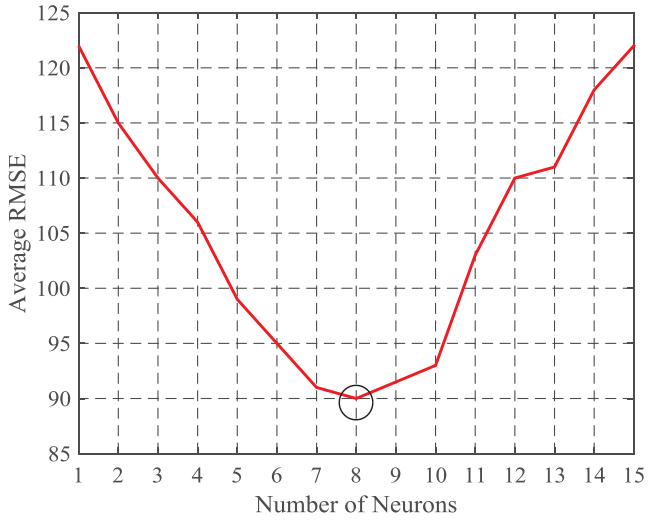

Fig. 4. Neuron-Validation for a Single-Hidden-Layered RBPNN Model.

approach resembled that of the single layered RBPNN model. However, the plot generated in this case was a heat map since there are two axes; a first hidden layer and a second hidden layer. This posed an extreme computation expense due to the presence of three iterations; therefore, the maximum number of neurons was capped at 20 neurons. Fig. 5 shows a thermal map composed of two hidden layers with varying neurons that range from 1 to 20 neurons. Similar to the single hidden layered model, ten iterations were executed for every neuron added in each layer. As a result, an RBPNN with 17 neurons in the first hidden layer and one neuron in the second hidden layer demonstrated the lowest average RMSE compared to the rest of the model architectures.

5.2. Employing the neural interpretation diagrams

After selecting the number of layers and neurons for an efficient RBPNN, the NID tool was employed within the model as shown in Fig. 6(a) and (b). As previously stated, the large number of wires and inputs make it difficult to extract the exact parameters that have contributed to the NID. Therefore, the Olden histograms, shown in Fig. 6(c) and (d), were generated to represent the total weights as a function of the relative importance. In this study, the first NID with all of the parameters was used to determine the variables with negative importance and the Olden histogram was used to quantify the importance in terms of a percentage, as shown in Fig. 6(a) and (c). As a result, the length, longitudinal steel reinforcement and yield strength were the parameters that demonstrated negative relative importance, whereas the rest of parameters yielded positive relative importance to the model. Afterwards, the selected independent parameters were employed within another NID tool for validation purposes. It has been observed from Fig. 6(b) and (d) that the previously selected features have associated positively with the model. However, this does not imply that all of the selected parameters consist of only blue wires radiating outwards, it means that the weighted average of the red and blue wires yielded positive outcomes. It is also worth mentioning that the majority of the FRP properties exhibited the highest relative importance within the model, which is intuitive since the shear capacity of FRP should depend mostly on its own properties.

5.3. Implementation of recursive feature elimination

While the implementations of NIDs and Olden histograms were useful approaches in investigating the parameters that contributed to the RBPNN model, this study also presented the implementation of the RFE algorithm to emphasize and validate the consistency of these

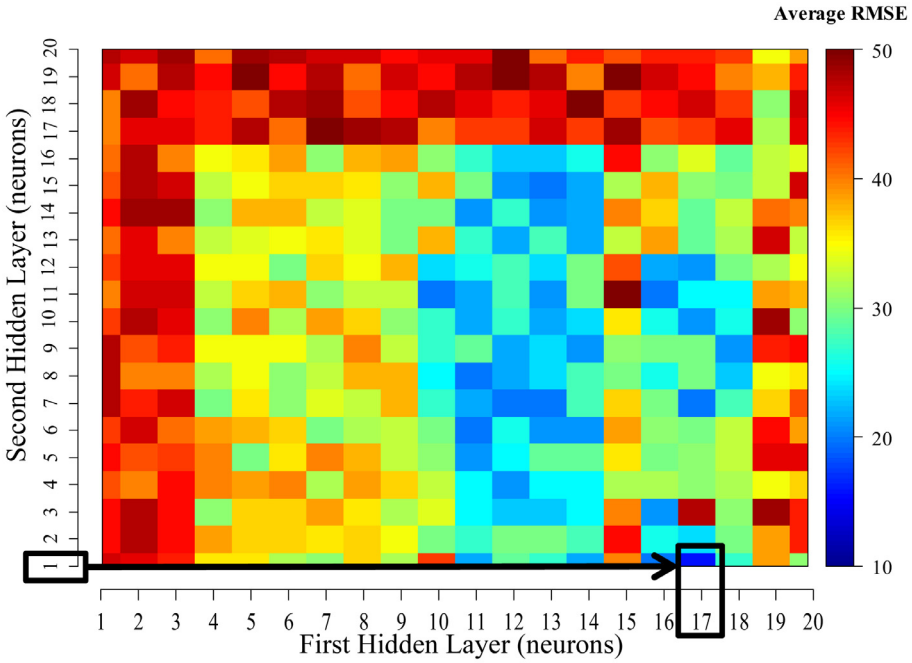

Fig. 5. Neuron-Validation for a Double-Hidden-Layered RBPNN Model.

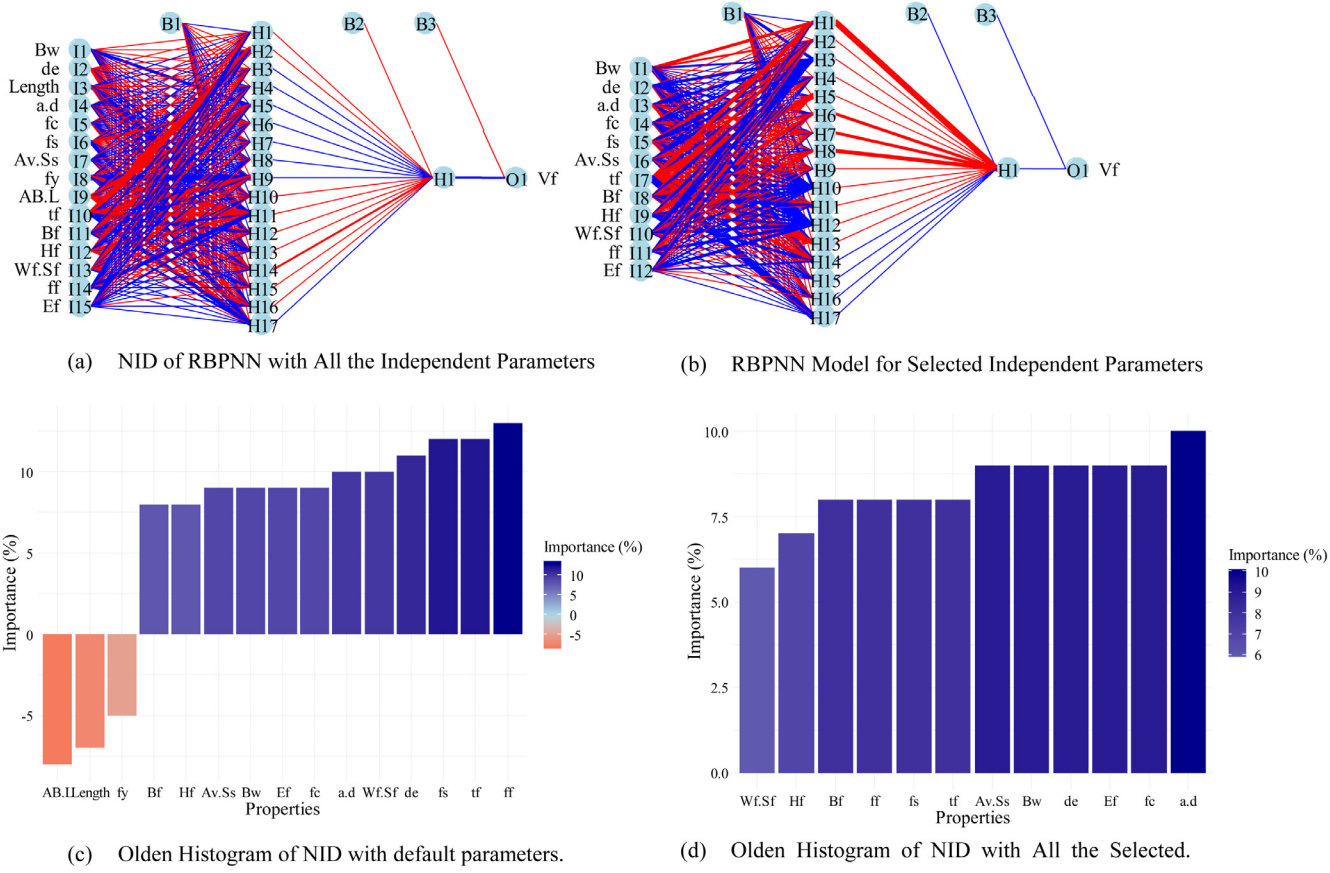

(a) NID of RBPNN with All the Independent Parameters

(b) RBPNN Model for Selected Independent Parameters

(c) Olden Histogram of NID with default parameters.

(d) Olden Histogram of NID with All the Selected.

Fig. 6. NID and Olden Histogram for RBPNN with All the Independent Parameters.

selections. The RFE tool was employed within the validated RBPNN model multiple times since the tool randomly appends the parameters until a significant rise in error is evident. Fig. 7 shows the most repeated selections in the form of a ranking system where the model terminated at a minimum RMSE value of 14.43 kN was achieved. Afterwards, the RFE algorithm detected a large marginal RMSE and terminated the analysis. Finally, the input parameters selected by both previously employed ML techniques were: beam width (Bw), effective depth of beam (deff), shear span-to-depth ratio (a/d), compressive strength of concrete (fc), yielding strength of stirrups (fy,s), Area of stirrups-to-

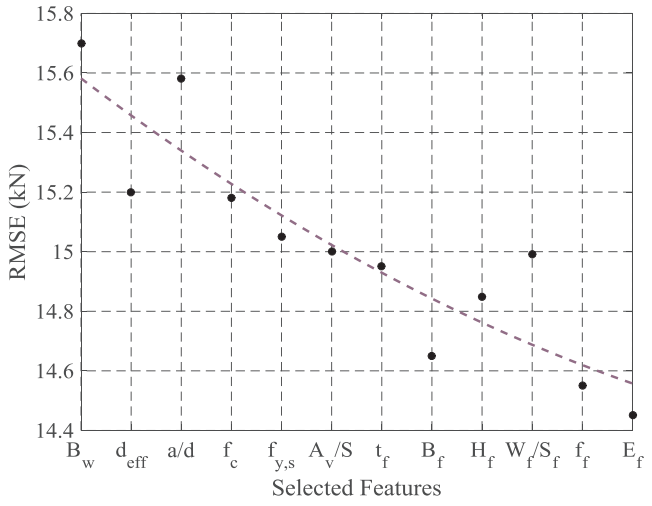

Fig. 7. RFE Plot of Selected Features.

spacing ratio (Av/S), thickness of FRP sheet (tf), width of FRP U-wrap (Bf), height of FRP strip (Hf), transverse FRP strip width-to-spacing ratio (Wf/Sf), and FRP elastic modulus (Ef). Further emphasis regarding the physical soundness of this selection is illustrated in the following section.

5.4. Physical cogency of the AI selection

This section presents a brief overview on the artificially selected parameters where the authors of this study referred to published literature involving these parameters. It was observed that analytical models developed by international design codes and standards like the ACI 440.2R-17 [45] and *fib*14 [46], as shown in Equations (5) and (6), used some of the parameters selected in this study to estimate the FRP shear capacity during real-life applications. It is worth mentioning that the variables in both Equations (5) and (6) are explained in the following sections. Moreover, experimental and numerical investigations were conducted to study the effect of most of these selected parameters on the FRP shear capacity of externally strengthened RC beams. [17,18,42,45–47]. Therefore, the NID and RFE was successful in identifying the main parameters that exhibit highly nonlinear relationships with the FRP shear capacity without the implementation of highly complicated concepts like the truss analogy.

$$(V_f)_{ACI} = \frac{A_{fv}\cdot f_{fe}\cdot(\sin\alpha + \cos\alpha)\cdot d_{fv}}{s} \quad (5)$$

$$(V_f)_{fib} = 0.9\cdot\varepsilon_{fd,e}\cdot E_f\cdot\rho_f\cdot b_w\cdot d\cdot(\cot\theta + \cot\alpha)\cdot\sin\alpha \quad (6)$$

6. Implementation of RBPNN modeling

6.1. RBPNN modeling with all default parameters

Predictions of the FRP shear capacity using default independent parameters were performed using the previously validated RBPNN model. The correlation coefficient (R^2) values were calculated during each randomly split set, where prediction versus experimental curves were generated to observe the fit during the analysis of each, as shown in Fig. 8(a)–(d). As a result, the analysis for training, validation, testing, and all sets yielded R^2 values of 0.705, 0.539, 0.615 and 0.668, respectively. Since the R^2 values of the training, validation, and testing sets were roughly similar, it was concluded that the RBPNN was not overfitting the points.

6.2. RBPNN with selected parameters

Similarly, another RBPNN model was employed to predict the FRP shear capacity using the selected features. Fig. 9(a)–(d) show the predicted versus experimental curves of the FRP shear capacities for the selected features per each set. It was observed that the correlation coefficient (R^2) values for the training, validating, testing and the combination of all sets were recorded as 0.874, 0.914, 0.961 and 0.885, respectively. Therefore, it was clearly observed that the model with the selected parameters outperformed the model with all default parameters, which strongly illustrates the benefits of implementing emerging ML toolboxes, specifically NID and RFE.

Furthermore, statistical measurements of both RBPNN models were calculated as shown in Table 3, where the R^2 and RMSE values, before and after selection, went from 0.668 to 0.885 and 16.6 kN to 8.1 kN, respectively.

6.3. Code comparison

The evaluation of FRP shear strength resistance was executed using three different design standards, mainly: the ACI 440.2R-17 [45], *fib*14 [46] and CNR-DT200 [47] FRP shear strength design standards. Table 4 shows the equations used to evaluate the contribution of FRP shear resistance based on the bonding configuration (i.e. U-wrap or side-bonded schemes).

These adopted numerical models yielded an array of shear strength values in which the predicted and experimental results were plotted against each other. Moreover, the ratio of the predicted-to-experimental shear strength was also evaluated and plotted for each design standard. These plots were compared with the plots produced by the ANN with selected features, as shown in Fig. 10. As a result, it was observed that the proposed ANN model was capable of estimating the FRP shear strength more accurately than the models that are available in the design standards. In addition, statistical measurements like the RMSE, R^2, standard deviation (SD), coefficient of variation (*COV*), and mean predicted-to-experimental shear strength ratio ($\mu_{P:E}$) were calculated to support this conclusion and are shown in Table 5. It is worth mentioning that the data points used to evaluate the shear strength of the specimens were obtained from the test segment (15% of the data points); hence, a more reliable comparison was made using data that was not trained or memorized by the proposed ANN (ANN_{test}).

7. Parametric study

It is clearly demonstrated that the implementation of NID and RFE tools, within the RBPNN model, yielded more accurate results in predicting the FRP shear capacity of the strengthened RC beams. As a result, a parametric study, using the developed RBPNN, was conducted to investigate the influence of variation of different parameters that affect the FRP shear strength. This also made the RBNN development more reliable by comparing the conclusions obtained from the parametric studies with the conclusions reported in the literature. In this section, the parametric study was divided into two separate investigations: (a) effect of FRP properties on FRP shear capacity; and (b) effect of transverse reinforcement (stirrups) on FRP shear capacity. The range of applicability of each parameter was assessed such that the parametric study explores the behavior of the specimens with realistic geometrical and mechanical properties. The varied parameters in the shear-strengthened RC beams abide by the codes and standards while providing the unique behavior of selected parameters within the RBPNN model. As a result, the two parametric studies were carefully designed to capture the behavior of shear strengthened beams.

The values of the parameters employed within the parametric study were selected within a domain bounded by the maximum and minimum values of experimental data shown in Table 1. For example, the widths of the beams were between 150 mm and 250 mm. The remaining

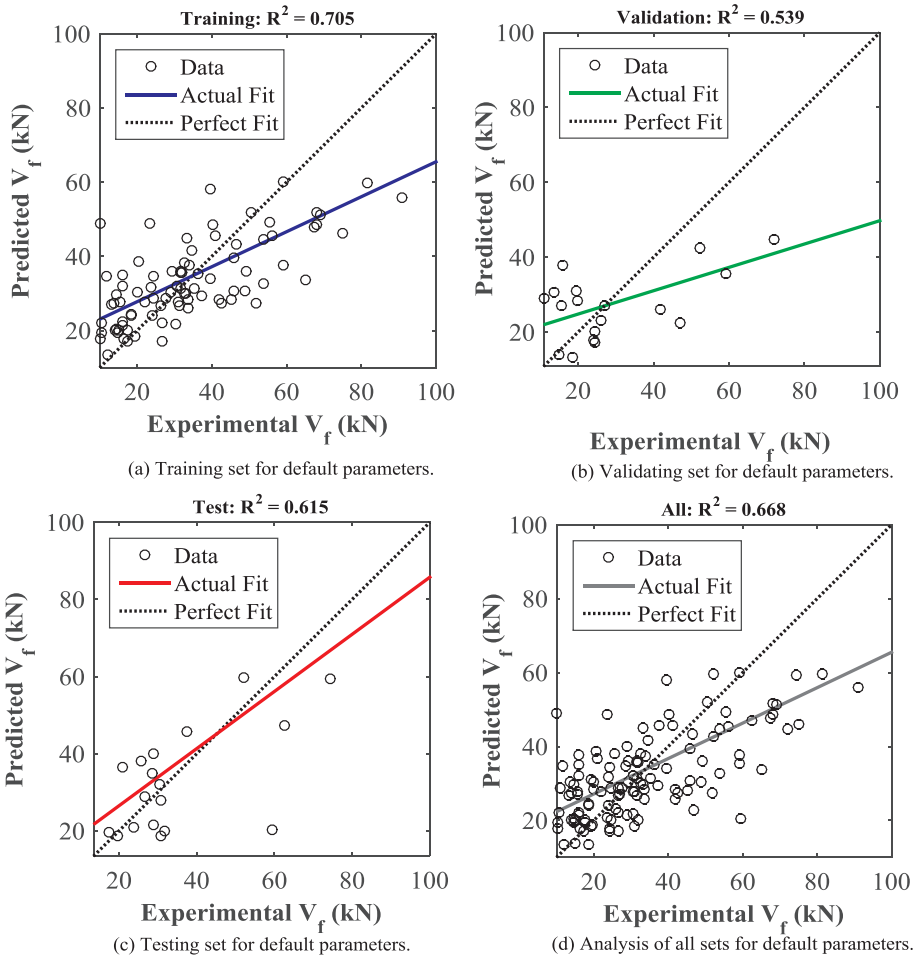

(a) Training set for default parameters.
(b) Validating set for default parameters.
(c) Testing set for default parameters.
(d) Analysis of all sets for default parameters.

Fig. 8. Predicted Versus Experimental Curves for FRP Shear Capacity using the Default Parameters.

parameters followed the same procedure except for A_v/S, f_f and E_f, whereby these parameters were a function of the type of design procedure used (A_v/S) or the type of FRP composite used (f_f and E_f). During the parametric study, the steel shear reinforcement depended on the minimum and maximum shear reinforcement limits imposed by the ACI 318-14 [44] design provisions as shown in Equations (7) and (8), where the final values are outlined in Table 6.

$$\left(\frac{A_v}{S}\right)_{\min} = \frac{1}{16}\sqrt{f'_c}\frac{b_w}{f_s} \geq \frac{0.33 b_w}{f_s} \tag{7}$$

$$\left(\frac{A_v}{S}\right)_{\max} = \frac{2A_b}{S_{\min}} \tag{8}$$

where f'_c is the concrete compressive strength, b_w is the width of the beam, f_s is the yield strength of the transverse reinforcement, A_b is the area of the bar used and S_{min} is the minimum spacing of stirrups taken as the greater of 25.4 mm or 1.33 times the aggregate size [44]; in this study, the minimum spacing and bar diameter used were 50 and 10 mm, respectively.

Furthermore, two types of FRP composites were used in this study; namely, CFRP and GFRP composites. These different composites were analyzed separately during the parametric study due to the different mechanical properties associated with both of these strengthening materials. This allowed the authors of this paper to assess the different responses accompanying the input of each composite within the RBPNN model. Since the data collection was focused primarily on both Side-Bonded (SB) and U-Wrapped (UW) FRP strengthening schemes, the parametric study accounted for both of these parameters separately to illustrate their underlying effect on the FRP shear capacity in externally strengthened RC beams. Table 7 shows the parameters of the studied specimens and the range of the parameters that are used as variables for the two conducted parametric studies. The values of area of stirrups-to-spacing ratio (A_v/S) were obtained from the database and were between the design limits evaluated using Equations (7) and (8). Similarly, the ultimate tensile strength and modulus of elasticity for both the CFRP and GFRP sheets were taken as the average values of their corresponding composites within the collected database. The parameters that were varied during the parametric studies were according to their median and mean values such that most of the properties of shear-strengthened RC beams were captured.

7.1. Effect of FRP properties on FRP shear capacity

The aim of this parametric study is to investigate the effect of varying the FRP thickness (t_f) and FRP strip width-to-spacing ratio (W_f/S_f) of the shear strength of RC beams strengthened with two different strengthening mechanisms: (a) SD and UW; (b) two different FRP materials (CFRP and GFRP). The FRP thickness (t_f) ranged between 0.1 and 0.3 and FRP strip width-to-spacing ratio (W_f/S_f) ranged between 0.25 and 1.0, while the area of stirrups-to-spacing ratio (A_v/S) fixed at 0.5, all other parameters are kept constant as shown in Table 7. This resulted in four conditions for the RC beam, mainly SB-CFRP, SB-GFRP, UW-CFRP and UW-GFRP.

Fig. 11(a) shows the effect of variation of CFRP thickness (t_f) and width-to-spacing ratio (W_f/S_f) on CFRP shear strength contribution (V_f) of RC beam strengthened with SB-CFRP. It is observed from Fig. 11(a) that an exponentially increasing relationship exists between the FRP shear resistance (V_f) and the width-to-spacing ratio (W_f/S_f). In addition,

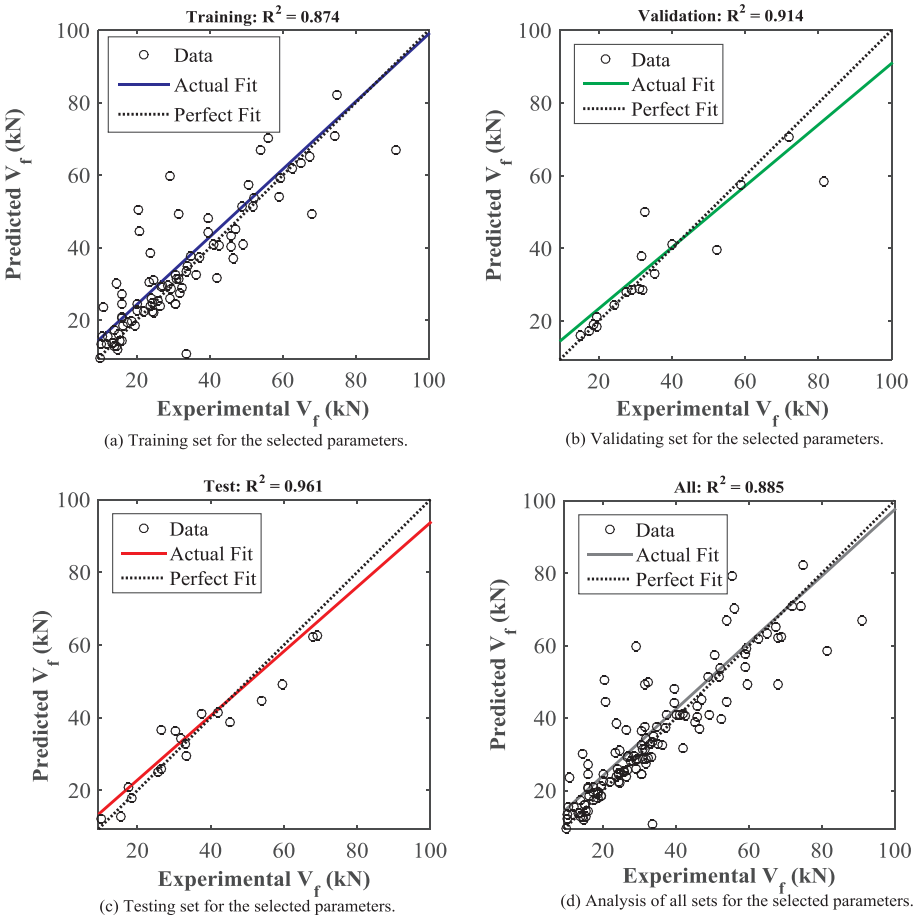

(a) Training set for the selected parameters.
(b) Validating set for the selected parameters.
(c) Testing set for the selected parameters.
(d) Analysis of all sets for the selected parameters.

Fig. 9. Predicted Versus Experimental Curves for FRP Shear Capacity using the Selected Parameters.

Table 3
Statistical Measurements for Both RBPNN Models.

Statistics Measurements	Before Selection	After Selection
r^2	0.668	0.885
RMSE (kN)	16.6	8.1

this behavior showed an increase (vertical shift) in the FRP shear resistance as the CFRP thickness increases from 0.1 mm to 0.3 mm. For example, the model with CFRP thickness of 0.1 mm and a width-to-spacing ratio of 0.25 achieved an FRP shear capacity of 57.6 kN, whereas the one with 0.2 mm CFRP thickness achieved an FRP shear capacity of 63.2 kN (i.e., an increase of 9.72%). This observation is consistent with the design standard formulae predictions where the FRP shear capacity is directly proportional to the FRP sheet thickness [48–50].

Fig. 11(b) shows the effect of variation of CFRP thickness (t_f) and width-to-spacing ratio (W_f/S_f) on CFRP shear strength contribution (V_f) of RC beam strengthened with U-Wrapped CFRP sheets (UW-CFRP). Similar exponentially increasing relationship exists as that of Fig. 11(a). Furthermore, changing the strengthening scheme to a U-Wrapped scheme enhanced the FRP shear capacity and demonstrated a larger vertical shift than that of SB-CFRP while still maintaining an exponential profile similar to that in Fig. 11(a). This demonstrated that the bottom segment of the U-shaped CFRP sheet enhanced the FRP shear resistance due to the increase in concrete confinement coupled with the flexural-shear interaction that were observed in other experimental investigations conducted by Hawileh et al. and Panda et al. [48,49]. For example, the model with CFRP thickness of 0.1 mm and a width-to-spacing ratio of 0.25 achieved a CFRP shear capacity of 63 kN, whereas the one with 0.2 mm CFRP thickness achieved an FRP shear capacity of 73.9 kN (i.e., an increase of 17.9%). It can be concluded that the increase in CFRP thickness has more influence in the CFRP shear capacity (17.9%) for U-Wapped strengthening mechanism as compared to the influence on Side-Bonded ones (9.72%).

Fig. 11(c) shows the effect of variation of GFRP thickness (t_f) and width-to-spacing ratio (W_f/S_f) on GFRP shear strength contribution (V_f) of RC beam strengthened with Side-Bonded GFRP sheets (SB-GFRP). It was observed that the relationship between the GFRP shear capacity and width-to-spacing ratio followed a bi-linear profile, by exhibiting a linear increase followed by a constant plateau, as shown in Fig. 11(c). In addition, this behavior showed an increase (vertical shift) in the GFRP shear resistance (V_f) as the GFRP thickness increases from 0.1 mm to 0.3 mm while maintaining the same bilinear profile. For example, at a thickness of 0.1 mm and a width-to-spacing ratio of 0.25, using a SB strengthening scheme, the FRP shear capacity reached 13.9 kN, whereas the section with a thickness of 0.2 mm and similar width-to-spacing ratio achieved GFRP shear capacity of 16.2 kN, as shown in Fig. 11(c) (i.e., an increase of 16.5%). The constant plateau portion of the graph presents a limit in the increase of the GFRP shear strength contribution (V_f). This phenomena occurred at certain width-to-spacing ratio of GFRP, roughly in the range of 0.60–0.65, after which no increase is observed in V_f with the increase in the width-to-spacing ratio as shown in Fig. 11(c). This conclusion is supported by an experimental and numerical study conducted by Banjara and Ramanjaneyulu [48] in which an increase in the thickness of GFRP-strengthened sections with homogeneously bonded sheets resulted in vertical shifts followed by constant FRP shear capacity.

Fig. 11(d) shows the effect of variation of GFRP thickness (t_f) and width-to-spacing ratio (W_f/S_f) on GFRP shear strength contribution (V_f)

Table 4
International design standards for shear strength of FRP.

Design Standards	Equations	where
ACI 440.2R-17 [43]	$v_f = \frac{A_{fv} f_{fe} (\sin\alpha + \cos\alpha) d_{fv}}{S_f}$	$A_{fv} = 2nt_f w_f$; $f_{fe} = \varepsilon_{fe} E_f$ $\varepsilon_{fe} = K_v \varepsilon_{fu} \le 0.004$ $K_v = \frac{k_1 k_2 L_e}{11,900\varepsilon_{fu}} \le 0.75$ $L_e = \frac{23,300}{(nt_f E_f)^{0.58}}$; $k_1 = \left(\frac{f_c}{27}\right)^{\frac{2}{3}}$ $K_2 = \begin{cases} \frac{d_{fv} - L_e}{d_{fv}}; & U-wrap \\ \frac{d_{fv} - 2L_e}{d_{fv}}; & Side\ Bonded \end{cases}$
*fib*14 [44]	$V_f = 0.9\varepsilon_{fe} E_f \rho_f b_w d(\cot\theta + \cot\alpha)\sin\alpha$	$\rho_f = \frac{2t_f w_f}{b_w S_f}$; $\varepsilon_{fe} = \min\left[0.65\left(\frac{f_c^{\frac{2}{3}}}{E_f \rho_f}\right)^{0.56} \times 10^{-3},\ 0.17\left(\frac{f_c^{\frac{2}{3}}}{E_f \rho_f}\right)^{0.3} \varepsilon_{fu}\right]$
CNR-DT200 [45]	$V_f = \begin{cases} \frac{0.9 d f_{fe} 2t_f (\cot\theta + \cot\alpha) w_f}{\gamma_{Rd} \rho_f}; & U-Wrap \\ \frac{A \min[0.9d, h_w] f_{fe} 2t_f \sin\alpha w_f}{\gamma_{Rd} \rho_f \sin\theta}; & Side\ Bounded \end{cases}$	$f_{fe} = \begin{cases} f_{fdd} \cdot \left[1 - \frac{1}{3} \cdot \frac{l_e \sin\alpha}{\min[0.9d, h_w]}\right] \\ f_{fdd} \cdot \frac{z_{rid,eq}}{\min[0.9d, h_w]} \cdot \left(1 - 0.6\sqrt{\frac{l_{eq}}{z_{rid,eq}}} \cdot\right) \end{cases}$

where V_f = the contribution of FRP shear resistance; d_{fv} = the depth of FRP strip from top of sheet to center of bottom reinforcement; n = the number of sheets used; t_f = the thickness of each FRP sheet; S_f = the center-to-center spacing between FRP sheets; θ = angle of concrete diagonal crack with respect to the beam's axis; α = the angle of FRP sheet; f_{fe} = the effective stress of FRP at failure; ε_{fe} = the FRP effective design strain; E_f = the elastic modulus of FRP. For further information regarding the calculation of V_f using CNR-DT200, refer to [47].

of RC beam strengthened with U-Wrapped GFRP sheets (UW-GFRP). The behavior of the UW-GFRP is similar to that of the SB-GFRP (i.e., bilinear profile). However, the increase (vertical shift) in the GFRP shear resistance (V_f) as the GFRP thickness increases from 0.1 mm to 0.3 mm while maintaining the same bilinear profile, is larger as shown in Fig. 11(d). This confirms that the increase in GFRP thickness influence the FRP shear strength contribution more in UW than in SB strength mechanism. For example, at GFRP thicknesses of both 0.1 mm

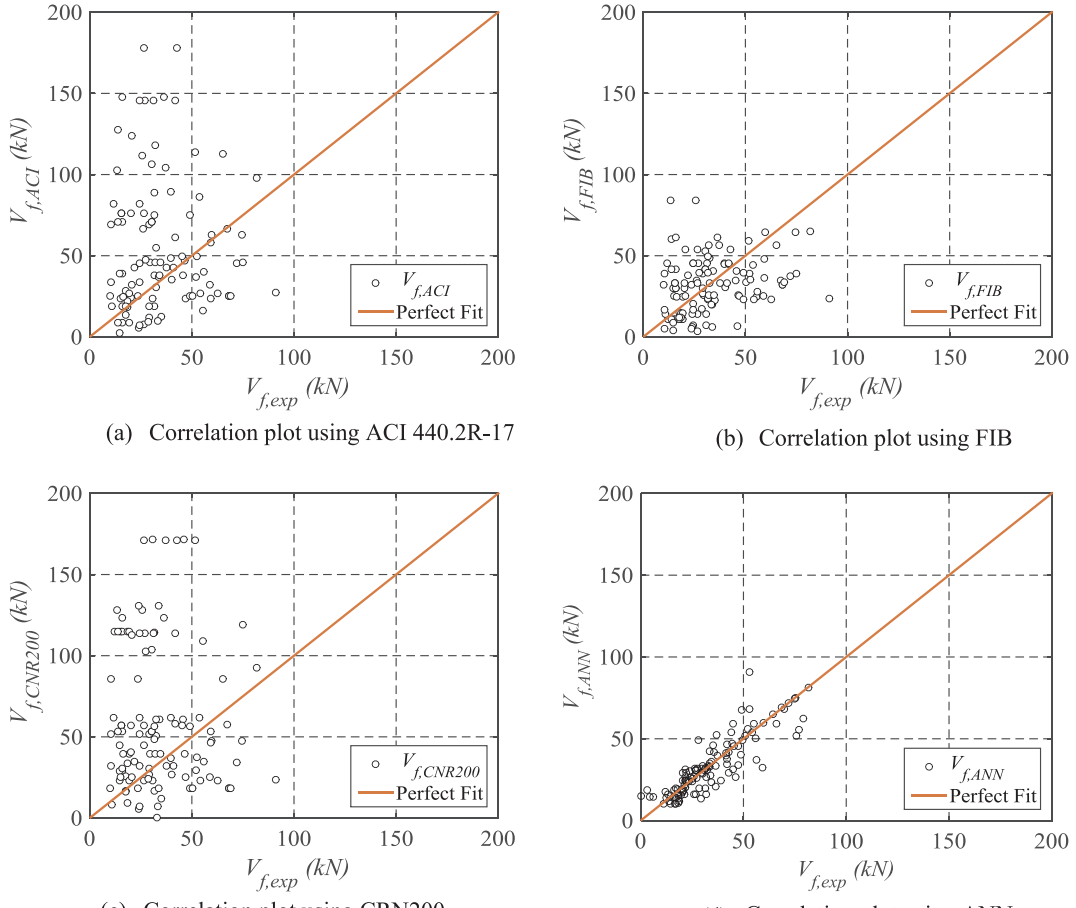

(a) Correlation plot using ACI 440.2R-17

(b) Correlation plot using FIB

(c) Correlation plot using CRN200

(d) Correlation plot using ANN

Fig. 10. Correlation and deviation plots.

Table 5
Statistical measurements of international design standards and proposed ANN.

Models	ACI 440.2R-17	*fib*14	CNR-DT200	ANN_{test}
RMSE (kN)	48.1	21.1	93.4	9.40
R^2	0.482	0.392	0.484	0.961
SD (kN)	43.9	20.88	82.5	8.80
COV (%)	90.7	52.8	91.6	28.6
$\mu_{P:E}$	1.775	1.18	2.85	1.06

and 0.2 mm, with width-to-spacing ratio of 0.25, both sections achieved FRP shear capacities of 17.3 kN and 23.4 kN (i.e., an increase of 37.0%).

7.2. Effect of internal transverse reinforcement (stirrups) on FRP shear capacity

The FRP strip width-to-spacing ratio ranged between 0.25 (spaced strips) to 1.0 (longitudinally homogenous sheet) such that these values were within the range prescribed in Table 2. Low amounts of internal transverse reinforcement (stirrups) were used to simulate a shear deficient RC beam during the parametric study as per the maximum and minimum transverse reinforcement prescribed by ACI 318-14 [44] and presented in Table 6. Finally, the mechanical properties of steel, concrete and FRP composites were taken as the average values in Table 2.

Fig. 12(a) shows the effect of variation of the internal transverse reinforcement, where the area of stirrups-to-spacing ratio (A_v/S) and CFRP strip width-to-spacing ratio (W_f/S_f) were varied based on a side-bonded CFRP scheme (SB-CFRP). It is observed from Fig. 12(a) that a slowly increasing parabolic relationship exists between the FRP shear resistance (V_f) and the stirrups-to-spacing ratio (A_v/S), accompanied by an increase (vertical shift) in the FRP shear strength contribution as the width-to-spacing ratio (W_f/S_f) increases from 0.25 to 1. For example, the model with width-to-spacing ratio of 0.25 and a stirrups-to-spacing ratio of 0.25 achieved an FRP shear capacity of 56.1 kN, whereas the width-to-spacing ratio increased to 0.5 while making no changes to the other parameters, the model yielded an FRP shear capacity of 59.2 kN (i.e., an increase of 5.53%). However, when larger amounts of A_v/S are used, the slope of the graph begins to decline; indicating a reduction in shear strength contribution by CFRP as area of stirrups-to-spacing. Several researchers conducted experimental and numerical investigations and reported this conclusion [16,50].

Fig. 12(b) shows the effect of variation of the internal transverse reinforcement, where the area of stirrups-to-spacing ratio (A_v/S) and CFRP strip width-to-spacing ratio (W_f/S_f) were varied based on a U-Wrapped CFRP scheme (UW-CFRP). A similar slowly increasing parabolic relationship to that of Fig. 12(a) is observed. Furthermore, changing the strengthening scheme to a U-Wrapped scheme showed little enhancement to the FRP shear capacity with very similar vertical shifts as that of SB-CFRP.

Fig. 12(c) shows the effect of variation of the internal transverse reinforcement, where the area of stirrups-to-spacing ratio (A_v/S) and GFRP strip width-to-spacing ratio (W_f/S_f) were varied based on a side-bonded GFRP scheme (SB-GFRP). It was observed that the relationship between the GFRP shear capacity and width-to-spacing ratio followed a bi-linear profile for high GFRP strip width-to-spacing ratio (W_f/S_f) (i.e., exhibiting a linear increase followed by a constant plateau). However, at lower W_f/S_f values (i.e., 0.25 and 0.5) the curves seem to exhibit a parabolic profile similar to those of Fig. 12(a) and (b). All curves showed an increase (vertical shift) in the GFRP shear resistance (V_f) as the width-to-spacing ratio (W_f/S_f) increases from 0.25 to 1.0, as shown in Fig. 12(c).

Fig. 12(d) shows the effect of variation of the internal transverse reinforcement, where the area of stirrups-to-spacing ratio (A_v/S) and GFRP strip width-to-spacing ratio (W_f/S_f) were varied based on a U-Wrapped GFRP scheme (UW-GFRP). The behavior of the UW-GFRP is similar to that of the SB-GFRP; a combination of bilinear profiles for high GFRP strip width-to-spacing ratio (W_f/S_f) and parabolic for low W_f/S_f. The bilinear behavior indicated that for of width-to-spacing ratio (W_f/S_f) greater than 0.5, the contribution of CFRP to shear strength does not increase and peaks at area of stirrups-to-spacing ratio (A_v/S) in the range of 0.5–0.75 as shown in Fig. 12(c) and (d). It is observed from Fig. 12(d) that the additional surface area provided by the U-wrap scheme accelerated the rate at which the GFRP shear strength contribution reached its limit as a function of A_v/S.

8. Summary and conclusions

In this study, a large database consisting of the mechanical and geometric properties of a shear-retrofitted RC beam was collected and analyzed using a RBPNN together with ML techniques such as RFE and NID. These ML techniques were used to construct a simpler network with fewer input parameters than the original one whereby the modified model yielding more accurate predictions than that of the original one. Furthermore, a parametric study was carried out to investigate the effect of different parameters on the shear capacity of FRP-strengthened RC beams. The model is consistent with previously conducted experimental studies. The following conclusions have been drawn from this study:

- RBPNN used with RFE and NID has proven to be an efficient approach in identifying the variables that strongly associated with the model.
- The RBPNN with the selected features was capable of predicting the FRP shear capacity more accurately (r^2 = 0.89; RMSE = 8.1 kN) than the RBPNN with all original features (r^2 = 0.67; RMSE = 16.6 kN).
- For the testing data, the RBPNN with the selected features outperformed all considered international code predictions by far with r^2 = 0.96 compared to ACI with r^2 = 0.48, *fib*14 with r^2 = 0.39 and CNR-DT200 with r^2 = 0.48.
- The parametric study explored the influence of a wide range of parameters on the FRP shear strength contribution. Such wide range of parameters cannot be easily covered by experimental investigations. The trends and behavior of the studied RC beams corroborated very well with the available experimental investigation results.
- For RC Beams strengthened with CFRP (UW or SB), the relationship between the FRP shear strength contribution and the FRP strip width-to-spacing ratio (W_f/S_f) is positively exponential for both SB and UW strengthening schemes. Slight increase in slope was evident when strengthening scheme changed from SB to UW.
- For RC Beams strengthened with GFRP (UW or SB), there is an optimum width-to-spacing ratio (W_f/S_f) for each FRP fiber thickness beyond which the FRP shear strength contribution (V_f) will not increase. The optimum FRP strip width-to-spacing ratio ranged

Table 6
Section properties for calculating reinforcement limits in the parametric study.

d_b (mm)	S_{min} (mm)	b_w (mm)	f_c (MPa)	f_s (MPa)	$\left(\frac{A_v}{S}\right)_{min}\left(\frac{mm^2}{mm}\right)$	$\left(\frac{A_v}{S}\right)_{max}\left(\frac{mm^2}{mm}\right)$
10	50	150	30	400	0.128	3.14

Table 7
Properties of shear strengthened RC beams investigated in this parametric study.

Parameter Description	Symbol (unit)	Side-Bonded (SD)		U-Wrapped (UW)	
		CFRP	GFRP	CFRP	GFRP
Beam width	b_w (mm)	150	150	150	150
Beam effective depth	d_e (mm)	300	300	300	300
Shear span-to-depth ratio	a/d	2.5	2.5	2.5	2.5
Concrete compressive strength	f_c (MPa)	30	30	30	30
Steel yield strength	f_y (MPa)	400	400	400	400
FRP strength	f_f (MPa)	3900	510	3900	510
FRP Modulus of elasticity	E_f (GPa)	230	24.2	230	24.2
FRP width	b_f (mm)	N/A	N/A	150	150
FRP height	h_f (mm)	300	300	450	450
FRP strip width-to-spacing ratio	W_f/S_f	0.25–1	0.25–1	0.25–1	0.25–1
FRP thickness	t_f (mm)	0.1–0.3 or 0.2	0.1–0.3 or 0.2	0.1–0.3 or 0.2	0.1–0.3 or 0.2
Area of stirrups-to-spacing ratio	A_v/S	0.5 or 0.25–1	0.5 or 0.25–1	0.5 or 0.25–1	0.5 or 0.25–1

between 0.5 and 0.75 for both SB and UW strengthening schemes.

- For RC Beams strengthened with CFRP (UW or SB), the relationship between the FRP shear strength contribution and the area of stirrups-to-spacing ratio (A_v/S) is positively parabolic for both SB and UW strengthening schemes. Significant increase in slope was evident when strengthening scheme changed from SB to UW.
- For RC Beams strengthened with GFRP (U-Wrapped or Side-Bonded) there is optimum area of stirrups-to-spacing ratio (A_v/S) for FRP strip width-to-spacing ratio (W_f/S_f) greater than or equal to 0.75; beyond which the FRP shear strength contribution (V_f) will not increase. The optimum A_v/S ratio is 0.50–0.75 for both SB and UW strengthening schemes.
- Using UW in both CFRP and GFRP sheets added an extra vertical shift due to the concrete confinement and flexural-shear interaction reported in other studies, indicating the consistency of the RBPNN with experimental investigations.

Declaration of Competing Interest

The authors declare that they have no known competing financial

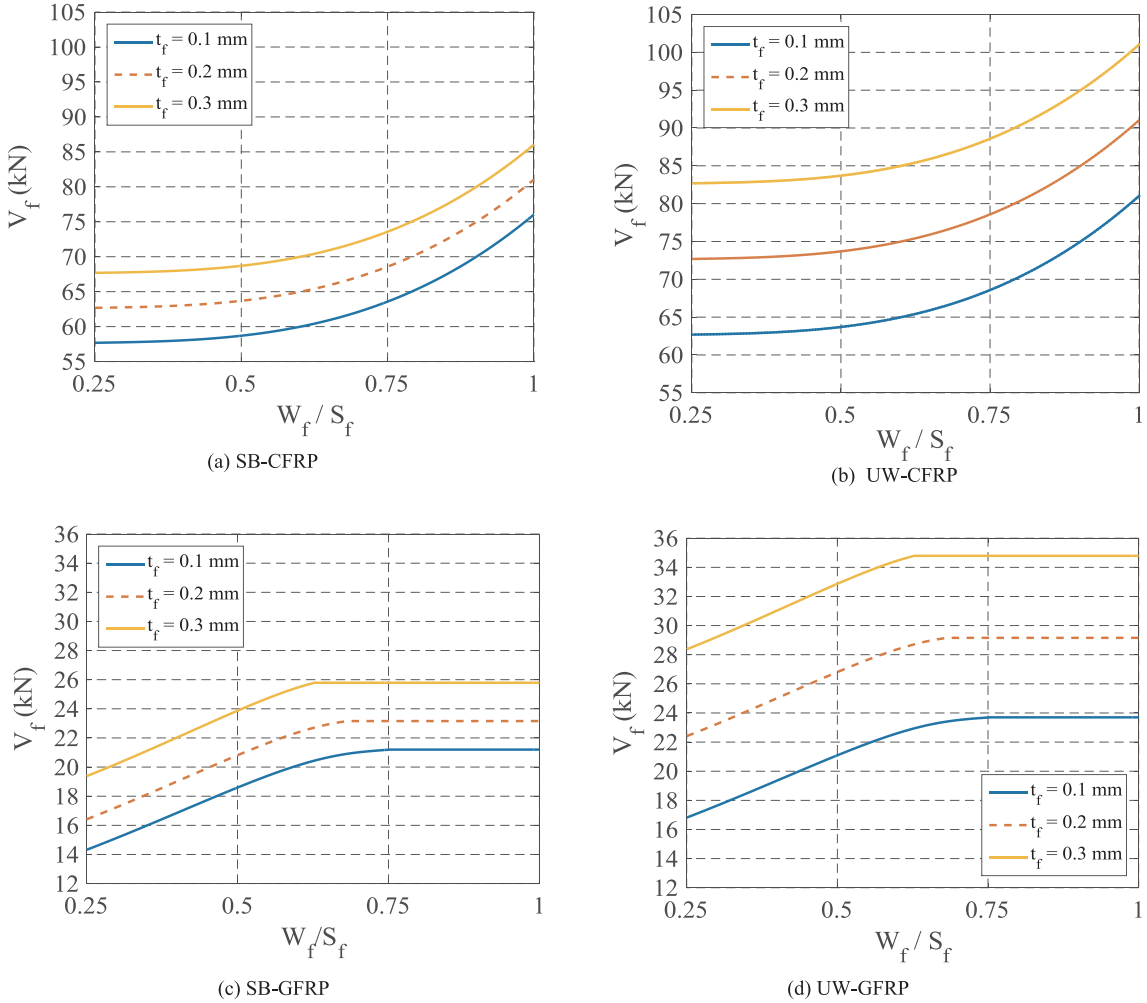

(a) SB-CFRP (b) UW-CFRP

(c) SB-GFRP (d) UW-GFRP

Fig. 11. Parametric Study on the Effect of FRP Properties on the FRP Shear Capacity.

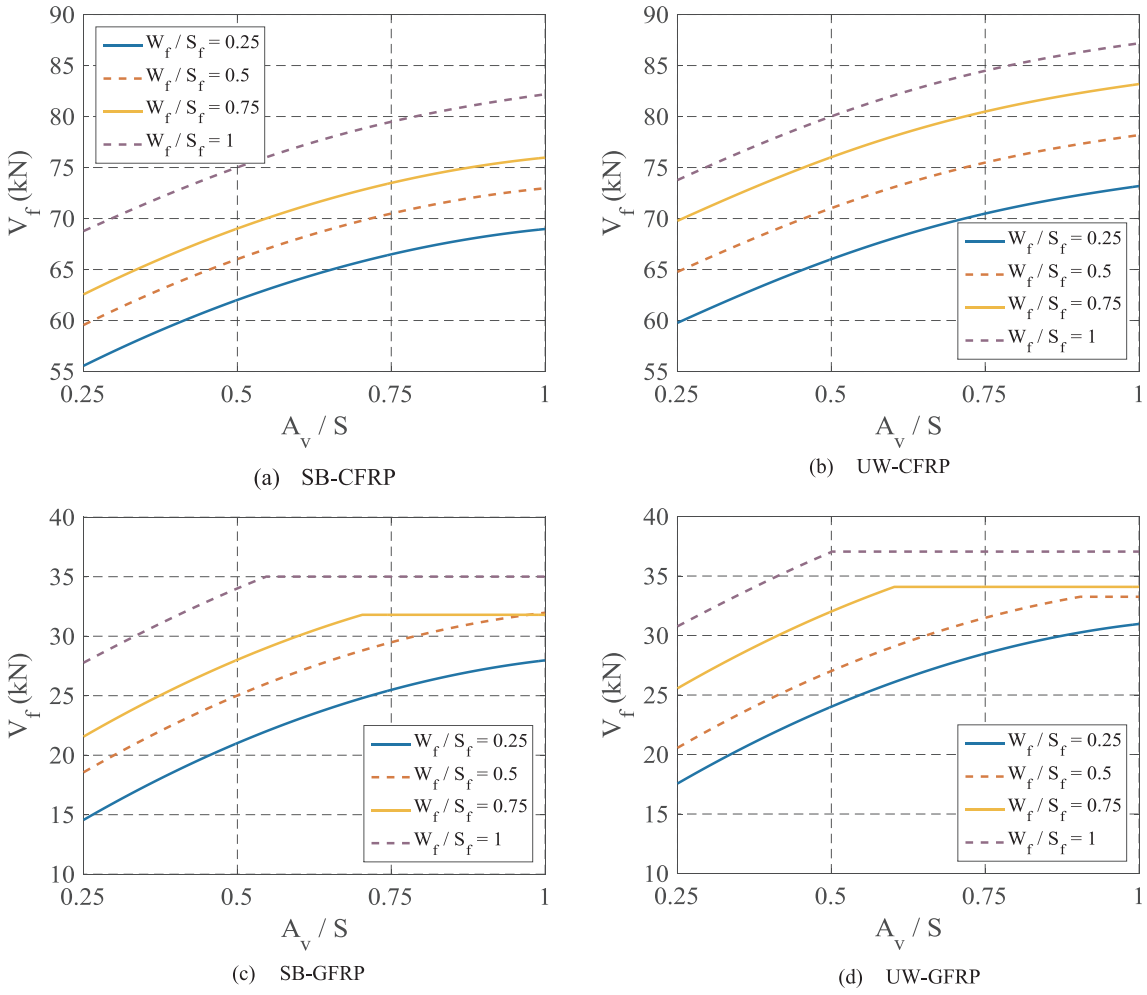

Fig. 12. Parametric Study on the Effect of ITR on the FRP Shear Capacity.

interests or personal relationships that could have appeared to influence the work reported in this paper.

Acknowledgments

The support for the research presented in this paper had been provided by Riad Sadek Endowed Chair in Civil Engineering at the American University of Sharjah. The support is gratefully appreciated and acknowledged. The views and conclusions, expressed or implied, in this study are those of the authors and should not be interpreted as those of the donor or the institution.

References

[1] Pham TM, Hadi MNS. Confinement model for FRP confined normal- and high-strength concrete circular columns. Constr Build Mater 2014;69:83–90.
[2] Jalal M, Ramezanianpour AA. Strength enhancement modeling of concrete cylinders confined with CFRP composites using artificial neural networks. Compos Part B Eng 2012;43(8):2990–3000.
[3] Hawileh RA, Rasheed HA, Abdalla JA, Al-Tamimi AK. Behavior of reinforced concrete beams strengthened with externally bonded hybrid fiber reinforced polymer systems. Mater Des Jan. 2014;53:972–82.
[4] Al-Tamimi AK, Hawileh RA, Abdalla JA, Rasheed HA. Effects of ratio of CFRP plate length to shear span and end anchorage on flexural behavior of SCC RC beams. J Compos Constr Dec. 2011;15(6):908–19.
[5] Ali A, Abdalla J, Hawileh R, Galal K. CFRP mechanical anchorage for externally strengthened RC beams under flexure. Phys Procedia 2014;55:10–6.
[6] Naser M, Hawileh R, Abdalla JA, Al-Tamimi A. Bond behavior of CFRP cured laminates: experimental and numerical investigation. J Eng Mater Technol Mar. 2012;134(2):21002–9.
[7] Chen GM, Teng JG, Chen JF. Process of debonding in RC beams shear-strengthened with FRP U-strips or side strips. Int J Solids Struct 2012;49(10):1266–82.
[8] Choi E, Utui N, Kim HS. Experimental and analytical investigations on debonding of hybrid FRPs for flexural strengthening of RC beams. Compos Part B Eng 2013;45(1):248–56.
[9] Abdalla JA, Abu-Obeidah AS, Hawileh RA, Rasheed HA. Shear strengthening of reinforced concrete beams using externally-bonded aluminum alloy plates: an experimental study. Constr Build Mater 2016;128:24–37.
[10] Abu-Obeidah A, Hawileh RA, Abdalla JA. Finite element analysis of strengthened RC beams in shear with aluminum plates. Comput Struct 2015;147:36–46.
[11] Rasheed HA, Abdalla J, Hawileh R, Al-Tamimi AK. Flexural behavior of reinforced concrete beams strengthened with externally bonded aluminum alloy plates. Eng Struct 2017;147:473–85.
[12] Douier KA, Hawileh R, Abdalla JA. Behavior of RC beams externally strengthened with mortar bonded steel mesh. 2019 Advances in Science and Engineering Technology International Conferences (ASET). 2019. p. 1–3.
[13] Hawileh RA, Nawaz W, Abdalla JA. Flexural behavior of reinforced concrete beams externally strengthened with Hardwire steel-fiber sheets. Constr Build Mater 2018;172:562–73.
[14] Karam EC, Hawileh RA, El Maaddawy T, Abdalla JA. Experimental investigations of repair of pre-damaged steel-concrete composite beams using CFRP laminates and mechanical anchors. Thin-Walled Struct 2017;112:107–17.
[15] Salama ASD, Hawileh RA, Abdalla JA. Performance of externally strengthened RC beams with side-bonded CFRP sheets. Compos Struct 2019;212:281–90.
[16] Hawileh RA, Abdalla JA, Tanarslan MH, Naser MZ. Modeling of nonlinear cyclic response of shear-deficient RC T-beams strengthened with side bonded CFRP fabric strips. Comput Concr Apr. 2011;8(2):193–206.
[17] Chen GM, Teng JG, Chen JF. Shear strength model for FRP-strengthened RC beams with adverse FRP-steel interaction. J Compos Constr 2013;17(1):50–66.
[18] Colotti V, Swamy RN. Unified analytical approach for determining shear capacity of RC beams strengthened with FRP. Eng Struct 2011;33(3):827–42.
[19] Abdalla JA, Elsanosi A, Abdelwahab A. Modeling and simulation of shear resistance of R/C beams using artificial neural network. J Franklin Inst 2007;344(5):741–56.
[20] Abdalla JA, Attom MF, Hawileh R. Prediction of minimum factor of safety against slope failure in clayey soils using artificial neural network. Environ Earth Sci 2015;73(9):5463–77.
[21] Abdalla JA, Hawileh R. Modeling and simulation of low-cycle fatigue life of steel reinforcing bars using artificial neural network. J Franklin Inst

2011;348(7):1393–403.
[22] Stoffel M, Bamer F, Markert B. Artificial neural networks and intelligent finite elements in non-linear structural mechanics. Thin-Walled Struct 2018;131(June):102–6.
[23] Elshafey AA, Dawood N, Marzouk H, Haddara M. Crack width in concrete using artificial neural networks. Eng Struct 2013;52:676–86.
[24] Yusif ST, Al-Jurama MA. Modeling of ultimate load for R.C. beams strengthened with Carbon FRP using artificial neural networks. Al Rafdain Eng J 2010;18(6):28–41.
[25] Cascardi A, Micelli F, Aiello MA. An artificial neural networks model for the prediction of the compressive strength of FRP-confined concrete circular columns. Eng Struct 2017;140:199–208.
[26] Naderpour H, Kheyroddin A, Amiri GG. Prediction of FRP-confined compressive strength of concrete using artificial neural networks. Compos Struct 2010;92(12):2817–29.
[27] Cevik A, Guzelbey IH. Neural network modeling of strength enhancement for CFRP confined concrete cylinders. Build Environ 2008;43(5):751–63.
[28] Mansouri I, Kisi O. Prediction of debonding strength for masonry elements retrofitted with FRP composites using neuro fuzzy and neural network approaches. Compos Part B Eng 2015;70:247–55.
[29] Rodriguez-Galiano VF, Luque-Espinar JA, Chica-Olmo M, Mendes MP. Feature selection approaches for predictive modelling of groundwater nitrate pollution: an evaluation of filters, embedded and wrapper methods. Sci Total Environ 2018;624:661–72.
[30] Mozumder RA, Laskar AI. Prediction of unconfined compressive strength of geopolymer stabilized clayey soil using artificial neural network. Comput Geotech 2015;69:291–300.
[31] Abuodeh OR, Abdalla JA, Hawileh RA. Prediction of compressive strength of ultra-high performance concrete using SFS and ANN. International Conference on Modeling Simulation and Applied Optimization (ICMSAO'19). 2019. p. 1–5.
[32] Abuodeh OR, Abdalla JA, Hawileh RA. Predicting the shear capacity of FRP in shear strengthened RC beams using ANN and NID. 8th International Conference on Modeling Simulation and Applied Optimization (ICMSAO'19). 2019. p. 1–5.
[33] Riedmiller M. Advanced supervised learning in multi-layer perceptrons—from backpropagation to adaptive learning algorithms. Comput Stand Interfaces 1994;16(3):265–78.
[34] Özesmi SL, Özesmi U. An artificial neural network approach to spatial habitat modelling with interspecific interaction. Ecol Model 1999;116(1):15–31.
[35] Olden JD, Jackson DA. Illuminating the 'black box': a randomization approach for understanding variable contributions in artificial neural networks. Ecol Model 2002;154(1):135–50.
[36] Cai J, Luo J, Wang S, Yang S. Feature selection in machine learning: a new perspective. Neurocomputing 2018;300:70–9.
[37] Tanarslan HM, Secer M, Kumanlioglu A. An approach for estimating the capacity of RC beams strengthened in shear with FRP reinforcements using artificial neural networks. Constr Build Mater 2012;30:556–68.
[38] Naderpour H, Poursaeidi O, Ahmadi M. Shear resistance prediction of concrete beams reinforced by FRP bars using artificial neural networks. Meas J Int Meas Confed 2018;126(May):299–308.
[39] Adhikary BB, Mutsuyoshi H. Artificial neural networks for the prediction of shear capacity of steel plate strengthened RC beams. Constr Build Mater 2004;18(6):409–17.
[40] Perera R, Arteaga A, De Diego A. Artificial intelligence techniques for prediction of the capacity of RC beams strengthened in shear with external FRP reinforcement. Compos Struct 2010;92(5):1169–75.
[41] Perera R, Barchín M, Arteaga A, De Diego A. Prediction of the ultimate strength of reinforced concrete beams FRP-strengthened in shear using neural networks. Compos Part B Eng 2010;41(4):287–98.
[42] W. Li, X. Ren, C. Hu, "Artificial Neural Network Model for FRP Shear Contribution of RC Beams Strengthened with Externally Bonded FRP Composites BT - 4th Annual International Conference on Material Engineering and Application (ICMEA 2017).".
[43] Naderpour H, Alavi SA. A proposed model to estimate shear contribution of FRP in strengthened RC beams in terms of adaptive neuro-fuzzy inference system. Compos Struct 2017;170:215–27.
[44] ACI Committee 318, Building Code Requirements for Structural Concrete (ACI 318-14). Farmington Hills, Michigan (USA): American Concrete Institute, 2019.
[45] ACI Committee 440, Guide for the Design and Construction of Externally Bonded FRP Systems for Strengthening Concrete Structures. Farmington Hills, Michigan (USA): American Concrete Institute, 2017.
[46] F. bulletin 14, Externally bonded FRP reinforcement for RC structures. Lausanne, Switzerland: International Federation for Structural Concrete (fib), 2001.
[47] CNR-DT200, Guide for the design and construction of externally bonded FRP systems for strengthening existing structures. Rome, Italy: Italian National Research Council, 2004.
[48] Hawileh RA, Nawaz W, Abdalla JA, Saqan EI. Effect of flexural CFRP sheets on shear resistance of reinforced concrete beams. Compos Struct 2015;122:468–76.
[49] Panda KC, Bhattacharyya SK, Barai SV. Effect of transverse steel on the performance of RC T-beams strengthened in shear zone with GFRP sheet. Constr Build Mater 2013;41:79–90.
[50] Banjara NK, Ramanjaneyulu K. Experimental and numerical investigations on the performance evaluation of shear deficient and GFRP strengthened reinforced concrete beams. Constr Build Mater 2017;137:520–34.